List of Publications

1. **D. Das**, A. Dutta, P. Mondal, Interactions of the aquated forms of ruthenium(III) anticancer drugs with protein: A detailed Molecular docking and QM/MM investigation, *RSC Adv*., 2014, **4**, 60548–60556. (I.F- 3.708).
2. **D. Das**, P. Mondal, Interaction of ruthenium(II) antitumor complexes with d(ATATAT)$_2$ and d(GCGCGC)$_2$: A theoretical study, *New. J. Chem*., 2015, **39**, 2515-2522. (I.F- 3.159).
3. **D. Das**, A. Dutta, P. Mondal, Interaction of aquated form of ruthenium(III) anticancer complexes with normal and mismatch base pairs: A theoretical study. (communicated)
4. **D. Das**, P. Mondal, Interaction mechanism of aquated form of ruthenium(III) anticancer complexes with histidine and cysteine: A density functional theory study, (communicated).
5. **D. Das**, P. Mondal Quantum chemical studies on detail mechanism of nitrosylation of NAMI-A-HSA adduct, (communicated).
6. **D. Das**, P. Mondal A computational study on structure and reactivity of ruthenium(III) anticancer complexes and their interaction with protein, (communicated).
7. **D. Das**, P. Mondal, A theoretical study on the hydrolysis process of the ruthenium(III) anticancer complexes, (communicated).

Miscellaneous work

1. C. R. Bhattacharjee , C. Datta , G. Das, **D. Das**, P. Mondal , S. K. Prasad, D.S. S. Rao, Photoluminescent columnar zinc(II) bimetallomesogen of tridentate [ONO]-donor Schiff base ligand, *Liquid Crystals*, 2013, **40**, 942-950. (I.F.-2.349)
2. H. A. R. Pramanik, D. Das, P. C. Paul , P. Mondal, C. R. Bhattacharjee, Newer mixed ligand Schiff base complexes from aquo-N-(20-hydroxy acetophenone) glycinatocopper(II) as synthon: DFT, antimicrobial activity and molecular docking study, *J. Mol. Struct*., 2014, **1059**, 309–319. (I.F-1.585)
3. C. Datta, **D. Das**, P. Mondal, B. Chakraborty, M. Sengupta, C. R. Bhattacharjee, Novel water soluble neutral vanadium(IV)eantibiotic complex: Antioxidant, immunomodulatory and molecular docking studies, *E. J. Med. Chem*., 2015, **97**, 214-224. (I.F-

Paper presented in conferences and national seminar

Poster presentation

1. "Adsorption of O, O2 and CO on Neutral and Charged Gas Phase Pt4 Clusters: A Density Functional Study" at National Workshop on Soft materials Organized by Centre for Soft Matter, held at Department of Chemistry, Assam University, Silchar on 17th September 2011.
2. "Density functional theory study of structure and reactivity of some antioxidant polyphenols and it molecular docking analysis" at National Symposium on Current Trends in Computational Chemistry held at Department of Chemistry, North-Eastern Hill University, on 16th to 17th March 2012.
3. "Density functional theory baesd QSAR study of Ruthenium(II) antitumor drugs and their interactions with Xanthine Oxidoreductase" at International Conference on Material Science (ICMS-2013) held at Department of Physics, Tripura University, on 21st to 23rd February 2013.

Oral presentation

1. "Structure and Reactivity of Ruthenium (III) anticancer drugs and their interaction with Proteins: A Theoretical Study" at National Conference on Chemistry, Chemical Technology and Society" held at Department of Chemical Sciences, Tezpur University on 11th to 12th November 2011.

2. "Bipyridine and terpyridine derivatized benzene core as electron transporting materials for organic light emitting devices (OLED): A Density functional study" at National seminar on Emerging areas of Research and Development in Chemical Sciences in North East India held at Department of Chemistry and Physics, Srikishan Sarda College, Hailakandi on 16th to 18th October 2012.

NJC

PAPER

View Article Online
View Journal | View Issue

Cite this: *New J. Chem.*, 2015, **39**, 2515

Interaction of ruthenium(II) antitumor complexes with d(ATATAT)$_2$ and d(GCGCGC)$_2$: a theoretical study

Dharitri Das and Paritosh Mondal*

Interaction of three ruthenium(II) complexes of the type $[Ru(tmp)_2(dpq)]^{2+}$ (**I**), $[Ru(tmp)_2(dppz)]^{2+}$ (**II**) and $[Ru(tmp)_2(11,12\text{-dmdppz})]^{2+}$ (**III**) with two B-DNA hexamers of alternative AT and GC sequences, namely d(ATATAT)$_2$ and d(GCGCGC)$_2$ respectively, has been computationally investigated by using the molecular docking and two layer quantum mechanics/molecular mechanics hybrid method. Docking simulation reveals the intercalative minor groove binding mode of ruthenium complexes with DNA base pairs as well as their preferential binding to d(ATATAT)$_2$ over d(GCGCGC)$_2$. In addition, docking simulation reveals the greater binding affinity of complex **III** toward the DNA sequences compared to complexes **I** and **II**, which indicates that the methyl substituent effect of the intercalating ligand increases the binding affinity towards the DNA duplex. Binding energies of ruthenium complexes with DNA sequences obtained from two layer quantum mechanics/molecular mechanics calculations show higher stability of the **III**–DNA adduct as compared to the adducts of complexes **I** and **II** with DNA. The stability order for ruthenium(II) complexes with d(ATATAT)$_2$ and d(GCGCGC)$_2$ sequences is as follows: complex **III** > complex **II** > complex **I**. Thus molecular docking and quantum mechanics/molecular mechanics results suggest that intercalating ligands having substituent groups significantly increase the DNA binding affinity of the metal complexes.

Received (in Victoria, Australia) 24th November 2014,
Accepted 6th January 2015

DOI: 10.1039/c4nj02118e

www.rsc.org/njc

1. Introduction

DNA is an important cancer target in the design of novel chemotherapeutics to block the replication step in the cell cycle. Even though the inhibition of DNA replication is not new in cancer therapy, the use of novel chemical reagents is still desirable to improve the effects of treatment, particularly by reducing the occurrence of drug side effects and resistance.[1–3] Biological activity is due to the covalent and non-covalent interactions of transition metal complexes with DNA.[4,5] The last decade has seen a series of transition metal complexes that have been used as DNA cleaving agents.[6–12] However, DNA cleavage by polypyridyl ruthenium(II) complexes has been the focal point of several research studies. Ruthenium(II) polypyridyl complexes have received a great deal of attention because of their stability, ease of construction, chirality, opto-electronic properties, strong binding affinity to DNA and luminescence characteristics.[6–9,13] Barton *et al.*[14] were among the first group of researchers who had analyzed the interactions of positively charged transition metal complexes with DNA. $[Ru(phen)_3]^{2+}$ (binding constant of 10^3 M^{-1}) can bind to DNA through three non-covalent modes, namely electrostatic, hydrophobic or by partial intercalation of the phenanthroline ligand into DNA.[13] On the other hand, Eriksson *et al.* have reported that both Δ and Λ enantiomer of the $[Ru(phen)_3]^{2+}$ complex bind to DNA only through an intercalative mode.[15] Intercalative binding is defined as the non-covalent stacking interaction occurring due to the insertion of a planar heterocyclic aromatic ring between base pairs of the DNA double helix.[16] $[Ru(bpy)_2(dppz)]^{2+}$ (bpy = 2,2′-bipyridine) and $[Ru(phen)_2(dppz)]^{2+}$ (phen = 1,10-phenanthroline) are the prototype of DNA intercalators that contain a DNA intercalating ligand namely dipyrido[3,2-*a*:2′,3′-*c*]phenazine (dppz).[17,18] Based on a recent crystallographic study conducted in the Barton and Lincoln laboratory, the Δ-enantiomer of $[Ru(bpy)_2dppz]^{2+}$ has been found to intercalate into the minor groove at CG/CG and AT/AT, resulting in DNA cleavage.[19–22] The $[Ru(bpy)_2(dppz)]^{2+}$ displayed an extremely high affinity for CT DNA, having a binding constant of 10^6 M^{-1}, which suggested that an increase in the surface area of the bridging ligand can significantly increase the DNA binding affinity.[17] On the other hand, according to Hall *et al.* both Λ- and Δ-enantiomer of $[Ru(phen)_2dppz]^{2+}$ show intercalation from the minor groove of DNA.[23] Erkkila *et al.* have carried out a systematic study of *rac*-$[Ru(5,6\text{-dmp})_3]^{2+}$–*rac*-$[Ru(phen)_3]^{2+}$ complexes and observed that the presence of the 5,6-dimethyl-1,10-phenanthroline ligand enhances the binding

Department of Chemistry, Assam University, Silchar 788011, Assam, India. E-mail: paritos_au@yahoo.co.in

affinity of *rac*-$[Ru(5,6\text{-dmp})_3]^{2+}$ with DNA receptors compared to the *rac*-$[Ru(phen)_3]^{2+}$ complex.[24] On studying the binding affinity of several osmium(II) tris-complexes of methyl substituted and unsubstituted 1,10-phenanthrolines with DNA, Maruyama and co-workers reported that the $[Os(5,6\text{-dmp})_3]^{2+}$ complex exhibits a very high DNA binding affinity.[25] On the other hand, Lincoln and co-workers revealed that methyl substituents on the distant benzene ring of the dppz ligand in the $[Ru(phen)_2 11,12\text{-dmdppz}]^{2+}$ complex substantially increase the luminescence lifetimes and quantum yields when bound to DNA.[26] Rajendiran *et al.* studied the DNA binding mode of a series of ruthenium complexes of the type $[Ru(tmp)_2\text{–}(5,6\text{-dmp})_2\ (diimine)]^{2+}$ with different diimine ligands and demonstrated that complexes with methyl substituted diimine ligands bind to DNA more strongly than the other complexes.[27] Vilar *et al.* have reported that ligands containing substituents such as aromatic rings and cyclic amines play an important role in determining the DNA binding affinity.[28] The interaction between ruthenium polypyridyl complexes and DNA has been studied for the last thirty years[29–31] because of the light switching properties and photosensitizing reactions of these complexes[32,33] but their detailed mode of action at the molecular level is still lacking.[34] The present study focuses on the interaction of Ru(II) polypyridyl complexes of the type $[Ru(tmp)_2(diimine)]^{2+}$ with the DNA molecule in order to evaluate the information regarding the intercalative binding mode of the complexes with DNA receptors.

In principle, various techniques are available to understand the *in vitro* reversible binding of metal complexes to the double-helical DNA such as spectroscopy, voltammetry and quantum chemical calculations. Indeed, molecular mechanics with improved force fields[35,36] have been extensively used to analyze the structural, mechanistic and energetic properties of biomolecules. However, the molecular mechanics is not able to calculate the breaking or formation of chemical bonds. Therefore, quantum mechanical simulation has been considered for studying the interaction of biomolecules with small drug molecules. Quantum mechanical simulations can perfectly describe the hydrogen, ionic and covalent binding interactions. Unfortunately, quantum mechanical methods of high-quality are computationally very expensive and cannot be used directly for studying DNA. Hence, Morokuma and co-workers have developed a hybrid method (ONIOM) based on the combination of several theoretical approaches for large biomolecular systems.[37,38] ONIOM (our Own N-layer Integrated molecular Orbital molecular Mechanics) is a powerful and systematic method which divides the system into several layers. In the past few years, many researchers have utilized this powerful computational method in order to find out the stability and binding affinity of anticancer drug molecules with DNA and protein receptors.[39–44] Recently we have used this method to explore the interaction of drug molecules with protein receptors.[45] In this study, molecular docking and the ONIOM (QM/MM) method have been used to investigate the structural and energetic details of the DNA duplex with $[Ru(tmp)_2(dpq)]^{2+}$ (**I**), $[Ru(tmp)_2(dppz)]^{2+}$ (**II**) and $[Ru(tmp)_2(11,12\text{-dmdppz})]^{2+}$ (**III**) complexes. The mode of coordination of the ligands with Ru^{2+} is depicted in Scheme 1. In order to recognize the appropriate orientation of the metal complex in the binding site of DNA, in terms of energy, molecular docking simulations are taken up in an initial step and then quantum chemical calculations are performed using the two layer ONIOM method.

2. Computational details

2.1 Structure

The GAUSSIAN 09 program package[46] is employed to carry out density functional theory (DFT) calculations on all the ruthenium(II) complexes using the Becke's[47] three parameter hybrid exchange functional (B3) and the Lee–Yang–Parr correlation functional (LYP) (B3LYP).[48] The B3LYP functional has been used because it provides a good description of reaction profiles for transition metal complexes.[49] The LANL2DZ basis set[50] which describes the effective core potential of Wadt and Hay (Los Alamos ECP) on the ruthenium atom and the 6-311+G(d,p) basis set[51] for all the non-metal atoms have been used for ground state geometry optimization. The reason for using the LANL2DZ basis set is that it reduces the calculation time for molecules containing larger nuclei. The gas phase geometries of the ruthenium(II) complexes have been fully optimized using the restricted B3LYP method without imposing any symmetry constrains with tight

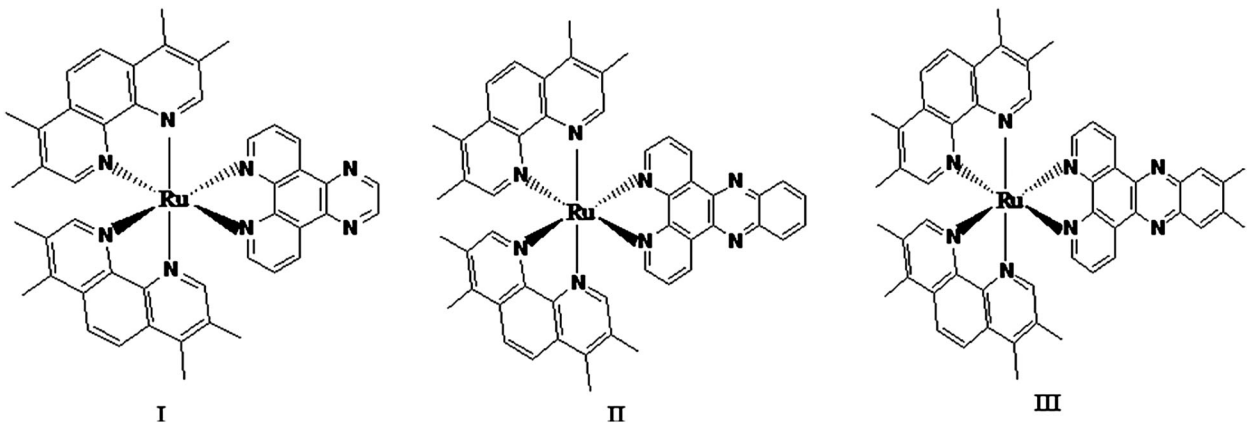

Scheme 1 Structure of ruthenium(II) complexes.

convergence criteria. Vibrational analysis has been performed at the same level of theory for achieving energy minimum.

2.2 Automated DNA–ruthenium complex docking

Molecular docking is an attractive scaffold in order to understand drug–DNA interactions for rational drug design and discovery. This method is extensively used for predicting ligand conformation and its orientation in the active site of the receptor. In our experiments, molecular docking studies of ruthenium(II) complexes (**I, II** and **III**) with the DNA duplex of sequence $d(ATATAT)_2$ and $d(GCGCGC)_2$ are performed in order to find out the binding affinity and appropriate orientation of the complexes inside the DNA groove by using the Auto Dock 4.2 program.[52] Auto Dock 4.2 is an interactive molecular graphics program utilized to study the drug–DNA interaction.[53] The first step of this study is to validate the docking method. The starting point is the 3D structure of a DNA duplex, $d(ATGCAT)_2$, which is co-crystallized with the native ligands *Λ*- and *Δ*-enantiomer of $[Ru(phen)_2dppz]^{2+}$ (PDB code: 4e87). The crystal structure of the DNA duplex $d(ATGCAT)_2$ is obtained from the Research Collaboratory for Structural Bioinformatics (RCSB) protein data bank whose conformation is generally B-type DNA with a low overall twist. For docking, the DNA structure in the pdb format is prepared using the structure preparation tool available in the Auto Dock Tools package version 1.5.4. All the water molecules and the native ligand have been removed from the crystal structure of DNA and then polar hydrogen atoms have been added for saturation; Gasteiger charges are computed and non-polar hydrogen atoms are merged. Then a grid box with a grid spacing of 0.375 Å and dimension of 60 × 60 × 60 points along *x*, *y* and *z* axes was built around the active site of DNA. This grid box carries the complete binding site of the DNA and provides enough space for the translational and rotational movement of the ligand. After that to test the validity of the docking procedure, a blind docking experiment is run on $[Ru(phen)_2dppz]^{2+}$ (*Δ*-enantiomer) by selecting step sizes of 2 Å for translation and 50° for rotation. The maximum number of energy evaluations are set to 25 000 and a maximum number of 27 000 GA operations are generated with an initial population of 150 individuals. The rates of gene mutation and crossover are set to 0.02 and 0.80, respectively. All other parameters are kept by default. The docking experiment described above is said to be valid because we obtained a similar orientation and position of the native ligand inside the DNA receptor as reported in the original X-ray crystal structure, available in the protein data bank (4e87) with an RMSD value 0.03 Å. The result of the validity experiment is shown in Fig. 1. All the studied ruthenium(II) complexes are docked with the same method described above.

2.3 Ruthenium complex–DNA interaction by using the QM/MM method

For performing ONIOM calculations we have considered the adduct formed between the native ligand and the DNA duplex $d(ATGCAT)_2$, as the reference point. Docking simulation shows that the native ligand intercalates into the 2nd and 3rd base pairs of DNA. Then, AT base pairs are replaced with GC base pairs from the $d(ATGCAT)_2$ sequence to obtain $d(GCGCGC)_2$ and the GC base

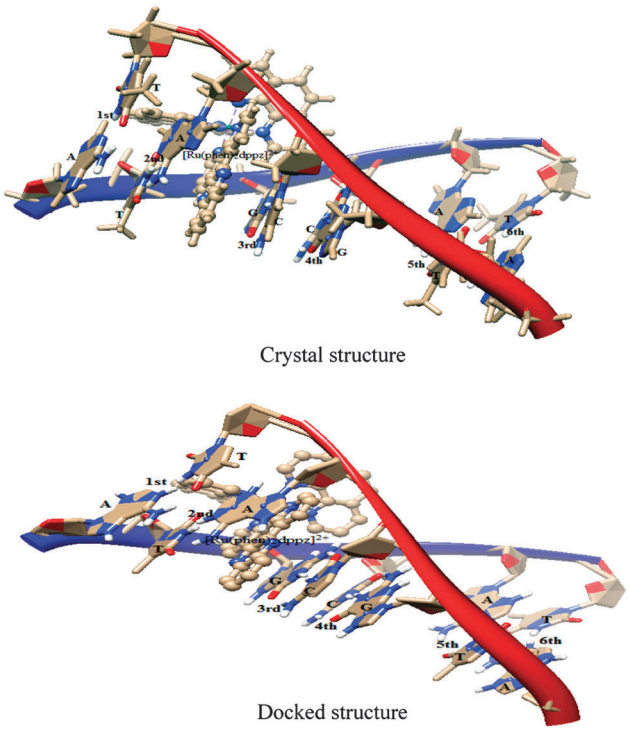

Fig. 1 Docked conformation of the native ligand $[Ru(phen)_2dppz]^{2+}$ as compared to the conformation of the ligand in the original crystal structure.

pair with the AT base pair to obtain the $d(ATATAT)_2$ duplex. The DNA sequences generated are subjected to optimization by treating AT–AT and GC–GC (2nd and 3rd) base pairs (high level) with QM and the remaining DNA bases and the sugar–phosphate backbone (low layer) with MM in order to get a minimized energy structure. The charges of both the layers are set to be 0. The RB3LYP functional with the 6-311+G(d,p) basis set is used for the QM layer while the UFF force field is used for the MM layer of the system.

Again docking simulation has been carried out on the ruthenium(II) complexes with energy minimized DNA structures namely $d(GCGCGC)_2$ and $d(ATATAT)_2$ and best docked structures of the complexes are selected for ONIOM calculations. The high level part (QM) includes the 2nd and 3rd base pairs of DNA along with the intercalated ruthenium complex. The charge of this layer is set to be +2. On the other hand, the remaining part of DNA, *i.e.* DNA bases and the sugar–phosphate backbone, is treated with MM and the charge of this is set to be 0. Finally, the whole structure is optimized using the two layer ONIOM method at the B3LYP/6-311+G(d,p): UFF (QM:MM) level. All the atoms in the MM layer are kept fixed at their crystallographic location during geometry optimization. In the two layer ONIOM method, the total energy (E_{ONIOM}) of the entire system is obtained from three independent energy calculations:

$$E^{ONIOM2} = E^{high}_{model\ system} + E^{low}_{real\ system} + E^{low}_{model\ system}$$

The real system contains the full geometry of the system and is considered as the MM layer while the model system contains the chemically most important (core) part of the system that is considered as the QM layer. This QM/MM computation

provides a close approximation of the energy value with the whole system calculated at a high level of theory.[54,55]

3. Results and discussion

3.1 Structural analysis of metal complexes

Significant optimized geometrical parameters and geometries of ruthenium complexes **I**, **II** and **III** evaluated in gas phase at the B3LYP level are presented in Table 1 and Fig. 2, respectively. In all the complexes, the Ru^{2+} ion is octahedrally coordinated involving four nitrogen atoms of the ancillary ligand (tmp) and two nitrogen atoms of the intercalating ligand (diimine). In complex **I**, the Ru–N1, Ru–N2, Ru–N3, Ru–N4, Ru–N5 and Ru–N6 bond lengths are calculated to be 2.113 Å, 2.116 Å, 2.116 Å, 2.115 Å, 2.106 Å and 2.096 Å, respectively, while Ru–N5 and Ru–N6 bond lengths are found to be shorter than Ru–N1, Ru–N2, Ru–N3 and Ru–N4 bond lengths, indicating the stronger coordination ability of the diimine ligand (intercalating) compared to the tmp ligands (ancillary ligand). The bond angles N1–Ru–N2, N3–Ru–N4 and N5–Ru–N6 of complex **I** are found to be 78.53°, 78.29° and 79.14°, respectively. As a consequence of this deviation of bond angles from 90°, the geometry about the ruthenium atom is distorted from the regular octahedral structure. Electronic structures of all the three ruthenium complexes are found to be similar. The dihedral angle, N2–N6–N5–N3 (or N3–N5–N6–N2), as obtained from DFT is in the range of 9.36°–9.48° forming a twisted conformation of diimine with respect to the tmp moieties. Theoretical calculations show that the diimine ligand of complexes **I**, **II** and **III** is essentially planar, having a dihedral angle (N6–C6–C5–N5) of −0.88°, −0.64° and −0.86°, respectively. The calculated geometrical parameters are in agreement with the similar complex $[Ru(dmp)_2(dppz)]^{2+}$ investigated using X-ray diffraction by Liu *et al.*[56]

3.2 Stability of the ruthenium complexes

The electronic properties of molecules can be determined from frontier molecular orbitals,[57] *i.e.*, the highest occupied molecular orbital (HOMO) and the lowest unoccupied molecular orbital (LUMO). DFT calculated LUMO and HOMO energies of the ruthenium complexes are listed in Table 2. A LUMO–HOMO energy separation of a chemical system is used to predict the kinetic stability and the relative reactivity pattern. A lower value of energy separation indicates higher reactivity and lower kinetic stability of the molecules.[58] According to Pearson, LUMO–HOMO energy separation represents the chemical hardness which is a reliable reactivity parameter to predict the stability of a molecule.[59] The maximum hardness principle states that the most stable molecule has the maximum hardness value.[60] It is observed from computational investigations that complex **III** has a higher value of the LUMO–HOMO energy gap, hence a higher chemical hardness value. Therefore, complex **III** is found to be more stable than the other two complexes.

Table 1 Bond distances (Å), bond angles (°) and dihedral angles (°) of ruthenium(II) complexes and X-ray data for $[Ru(dmp)_2(dppz)]^{2+}$

Geometrical parameters	Complex **I**	Complex **II**	Complex **III**	$[Ru(dmp)_2(dppz)]^{2+}$ (X-ray)
Ru–N1	2.113	2.114	2.113	2.110
Ru–N2	2.116	2.115	2.116	2.092
Ru–N3	2.116	2.116	2.116	2.096
Ru–N4	2.115	2.115	2.114	2.096
Ru–N5	2.106	2.106	2.106	2.073
Ru–N6	2.096	2.095	2.109	2.079
N1–Ru–N2	78.53	78.54	78.53	79.54
N3–Ru–N4	78.29	78.30	78.29	79.63
N5–Ru–N6	79.14	79.21	79.21	78.88
N2–N6–N5–N3	9.38	9.36	9.48	48.60
N3–N5–N6–N2	9.38	9.36	9.48	
N6–C6–C5–N5	−0.88	−0.64	−0.86	

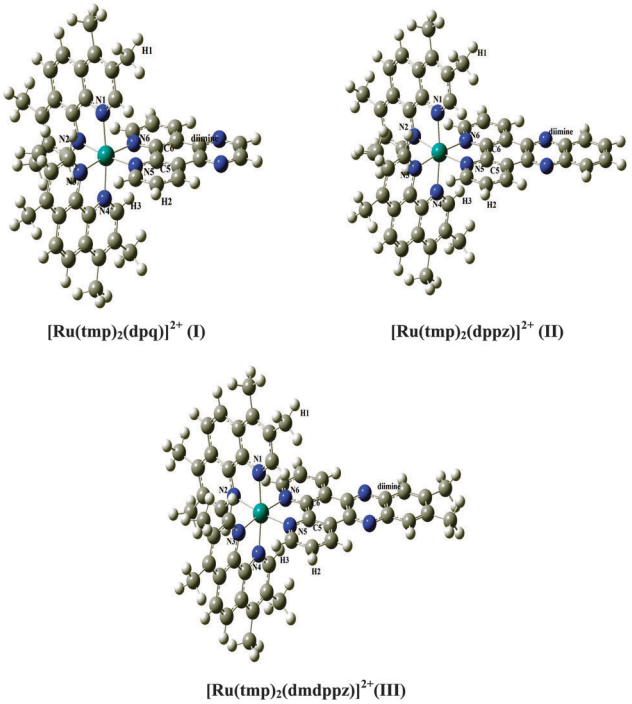

Fig. 2 Optimized geometries of ruthenium(II) complexes with appropriate numbering obtained from B3LYP/(LanL2DZ+6-311+G(d,p)) calculations.

Table 2 Energies of HOMO (E_H in eV) and LUMO (E_L in eV) and chemical hardness (η in eV) of three ruthenium(II) complexes

Complex	E_H	E_L	ΔE	η
I	−10.134	−6.818	3.316	1.658
II	−10.258	−6.896	3.362	1.681
III	−10.049	−6.653	3.396	1.698

Table 3 Free energy of binding (ΔG in kcal mol^{-1}), RMSD values and intrinsic binding constant (K_b in M^{-1}) of docked structures

Metal complex	$d(ATATAT)_2$		$d(GCGCGC)_2$		
	(ΔG)	RMSD	(ΔG)	RMSD	K_b experimental data
I	−10.88	0.02	−8.82	0.02	$3.0 \pm 0.2 \times 10^5$
II	−11.86	0.10	−10.64	0.14	$1.0 \pm 0.09 \times 10^6$
III	−11.99	0.05	−10.78	0.24	$6.0 \pm 0.3 \times 10^6$

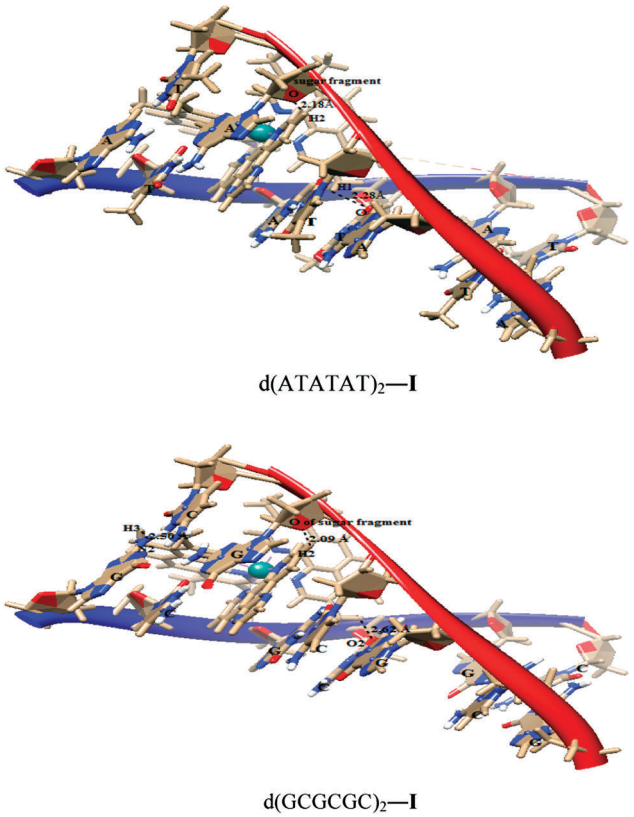

Fig. 3 Docked conformation of complex **I** with $d(ATATAT)_2$ and $d(GCGCGC)_2$ sequences.

3.3 Molecular docking study

Analysis of the molecular docking simulation shows that all the ruthenium complexes approach toward the gap between DNA minor grooves mainly through the diimine ligand. The relative binding energy, RMSD values and experimental binding constant (K_b in M^{-1}) values[27] of the studied complexes with DNA sequences ($d(ATATAT)_2$ and $d(GCGCGC)_2$) are reported in Table 3. Table 3 shows that all the complexes have RMSD values within the range of 0.02–0.24 Å. The relative binding energies of docked ruthenium complexes **I**, **II** and **III** with the $d(ATATAT)_2$ sequence are found to be −10.88, −11.86 and −11.99 kcal mol^{-1}, whereas for complexes with the $d(GCGCGC)_2$ sequence they are found to be −8.82, −10.64 and −10.78 kcal mol^{-1}, respectively. Higher negative values of binding energy reveal stronger interaction of drug molecules with DNA. Thus complex **III** is found to be more efficient towards the DNA target as compared to the other two complexes. This finding correlates well with the experimental DNA binding data reported in the literature.[27] Furthermore, it has been observed that most of the minor groove binding drug molecules prefer AT rich DNA sequences rather than GC rich DNA sequences and this preferential binding leads to a better van der Waals' interaction between the drug molecules and DNA functional groups.[61] Our docking result shows that the interaction energy of ruthenium complexes with AT sequences is found to be higher indicating the preferential binding of these complexes with the $d(ATATAT)_2$ sequence than with the $d(GCGCGC)_2$ sequence. The energetically most favorable docked conformation of complex **I** is shown in Fig. 3 and the possible binding interaction of ruthenium complexes with the receptor in terms of hydrogen bonding is presented in Table 4. In the minor groove of the $d(ATATAT)_2$ sequence, complex **I** binds to an O atom of the sugar fragment through the H2 atom of the diimine ligand at a distance of 2.18 Å. Another hydrogen bond between the H1 atom of the ruthenium complex and the O2 atom of thymine is observed at a distance of 2.28 Å. In $d(GCGCGC)_2$–**I**, one hydrogen bond between the H2 atom of the diimine ligand and the oxygen atom of the sugar fragment at a distance of 2.09 Å is noticed. On the other hand the tmp ligand of complex **I** forms hydrogen bonding with the N2 atom of guanine (2.50 Å) and the O2 atom of cytosine (2.62 Å). Similar types of bonding interactions have been observed for the docking structure of complexes **II** and **III** with respective DNA sequences which are summarized in Table 4.

3.4 QM/MM study

In this section binding energies of ruthenium complexes with DNA evaluated based on the QM/MM method are presented. For this purpose, the best docked structure of each ruthenium complex with the DNA duplexes $d(ATATAT)_2$ and $d(GCGCGC)_2$ has been taken for the two layer ONIOM (DFT/RB3LYP:UFF) study. Investigation of the whole DNA with the ligand by quantum mechanics (QM) is computationally very demanding. Hence, we have applied QM on the two base pairs along with the ruthenium complex and molecular mechanics (MM) for the remaining part of the system. Fig. 4 represents the optimized structures of two isolated hexanucleotide structures obtained

Table 4 Hydrogen bond interaction of three ruthenium(II) complexes with $d(ATATAT)_2$ and $d(GCGCGC)_2$ sequences evaluated by docking analysis

Complex	H-bond $d(ATATAT)_2$	Bond length (Å)	H-bond $d(GCGCGC)_2$	Bond length (Å)
I	H2 of diimine: O of the sugar fragment	2.18	H2 of diimine: O of the sugar fragment	2.09
	H1 of tmp: O2 of thymine	2.28	H1 of tmp: O2 of cytosine	2.62
			H3 of tmp: N2 of guanine	2.50
II	H2 of diimine: O of the sugar fragment	2.15	H2 of diimine: O of the sugar fragment	2.08
	H1 of tmp: O2 of thymine	2.18	H1 of tmp: O2 of cytosine	2.66
			H3 of tmp: N2 of guanine	2.50
III	H2 of diimine: O of the sugar fragment	2.15	H2 of diimine: O of the sugar fragment	2.05
	H1 of tmp: O2 of thymine	2.27	H1 of tmp: O2 of cytosine	2.65
			H3 of tmp: N2 of guanine	2.43

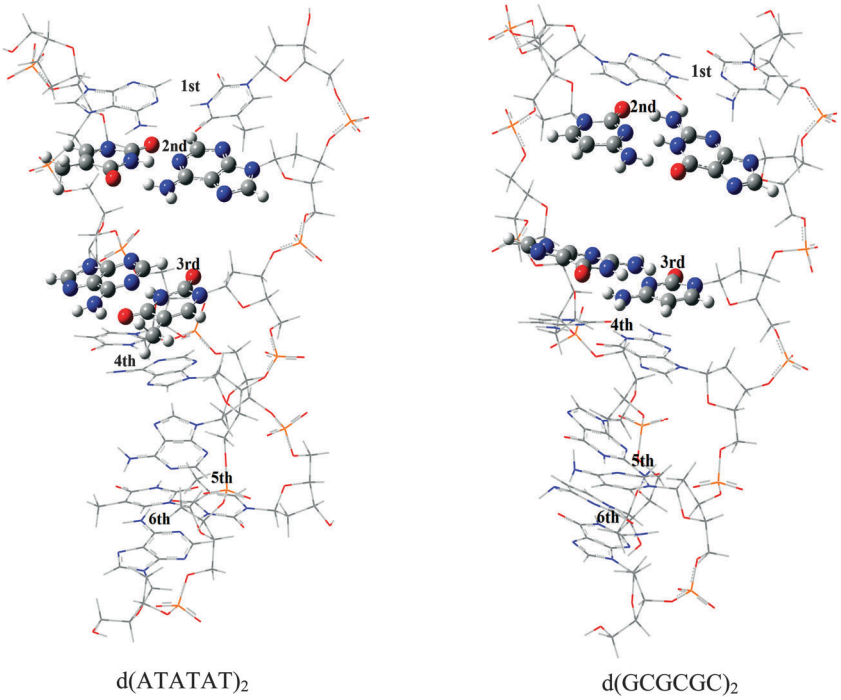

Fig. 4 Optimized geometry of $d(ATATAT)_2$ and $d(GCGCGC)_2$ obtained by using the two layer QM/MM method.

by using the two layer RB3LYP/UFF hybrid method. Results reveal that the QM/MM method can properly describe the AT and GC hydrogen bonding and π–π stacking interaction of base pairs. This result is attributable to the use of the universal force field in the MM low level layer that describes the entire DNA structure. In other terms, the universal force field prevents the unphysical occurrence of axial elongation of the stacked base pairs of the intercalation site at the time of energy minimization.

The optimized structures of $d(ATATAT)_2$–**I** and $d(GCGCGC)_2$–**I** adducts are shown in Fig. 5. From Fig. 4 and 5, it is seen that the intercalation of complex **I** induces a significant distortion in DNA duplexes, compared to the conformation of isolated hexanucleotides.

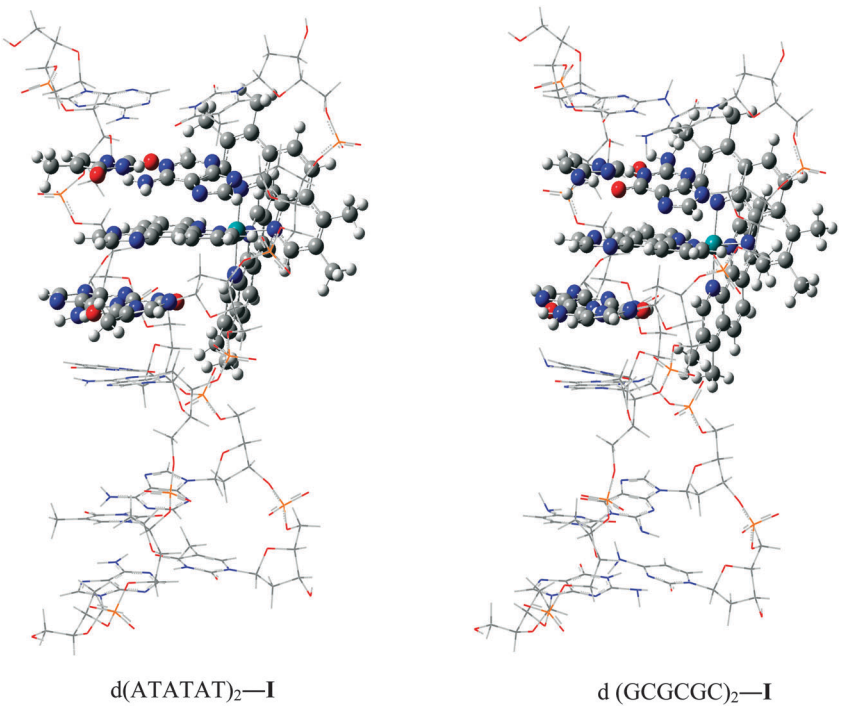

Fig. 5 Optimized geometries of $d(ATATAT)_2$–**I** and $d(GCGCGC)_2$–**I** adducts obtained by using the two layer QM/MM method.

Table 5 The structural parameters of two AT and/or GC base pairs of DNA in free as well in complex forms

Base pair	Base pair stacking distance (Å)	Base pair	Base pair stacking distance (Å)
Free AT–AT	3.35	Free GC–GC	3.35
AT–**I**	3.44	GC–**I**	3.48
AT–**II**	3.43	GC–**II**	3.42
AT–**III**	3.44	GC–**III**	3.49

Table 6 The calculated binding energy (ΔE in kcal mol^{-1}) of **I**, **II** and **III** with d(ATATAT)$_2$ and d(GCGCGC)$_2$ duplexes

	ΔE	
Complex	d(ATATAT)$_2$	d(GCGCGC)$_2$
I	222.072	−57.005
II	222.076	−53.527
III	222.452	44.802

For monitoring the deformation of DNA duplexes at the intercalation site, the relevant structural parameters are presented in Table 5. It is observed from Table 5 that on interaction of complex **I**, the average distance between two base pairs increases from 3.35 Å to 3.44 Å for d(ATATAT)$_2$ and to 3.48 Å for d(GCGCGC)$_2$, causing a larger axial elongation of the GC–GC base pair than the AT–AT base pair. Similar elongation of base pairs of the DNA duplex has also been observed for complexes **II** and **III**. Our calculation suggests that the diimine ligand of ruthenium complexes is situated within the narrower AT–AT region, indicating the preferential binding of the diimine moiety to the AT–AT region of DNA.

On the other hand, in order to compare the relative stability of the d(ATATAT)$_2$–**I**, d(ATATAT)$_2$–**II**, d(ATATAT)$_2$–**III** adducts with d(GCGCGC)$_2$–**I**, d(GCGCGC)$_2$–**II**, d(GCGCGC)$_2$–**III** adducts, we have evaluated the binding energy, ΔE:

$$\Delta E = E_{\text{DNA/Ru-complex}} - E_{\text{DNA}} - E_{\text{Ru-complex}}$$

$E_{\text{DNA/Ru-complex}}$ is the energy of the optimized DNA/Ru-complex, E_{DNA} is the energy of the optimized DNA duplex and the $E_{\text{Ru-complex}}$ is the energy of the optimized ruthenium complex. The binding energy values of all the ruthenium complexes with DNA are given in Table 6. Results shown in Table 6 lead us to conclude that the binding energy of ruthenium complexes with AT sequences is higher than that with GC sequences. Hence, complexes with AT sequences are more stable than those with corresponding GC sequences. Again, computed binding energies of adducts **III**–d(ATATAT)$_2$ and **III**–d(GCGCGC)$_2$ are evaluated to be 222.452 kcal mol^{-1} and 44.802 kcal mol^{-1}, respectively. These energy values are higher than those of the other adducts formed by complexes **I** and **II** with DNA. The higher stability of complex **III**–d(ATATAT)$_2$ may then be attributed to the higher π–π stacking and hydrophobic interaction of complex **III** with d(ATATAT)$_2$. Due to the presence of methyl substituents in the 11th and 12th position of the benzene ring, complex **III** exhibits higher interaction energy. These observations are in agreement with the experimental results reported by Rajendiran *et al.*[27] and Pyle *et al.*[62]

4. Conclusion

Systematic molecular docking and quantum mechanics/molecular mechanics calculations have been carried out on ruthenium(II) complexes **I**, **II** and **III** in order to evaluate their binding affinity and stability towards DNA receptors. Molecular docking simulation shows that the ruthenium(II) complexes interacted in the minor groove of DNA through the diimine ligand and prefer to bind to the d(ATATAT)$_2$ sequence. The docking result also reveals the higher binding affinity of complex **III** towards DNA receptors in comparison to complexes **I** and **II**. Again, two layer quantum mechanics/molecular mechanics calculations on d(ATATAT)$_2$/ruthenium(II) and d(GCGCGC)$_2$/ruthenium(II) adducts provide atomic level structural and energetic details on the intercalated ruthenium complexes. The interaction energy evaluated by quantum mechanics/molecular mechanics calculations suggests the highest stability of complex **III** with the d(ATATAT)$_2$ sequence. The higher interaction energies of ruthenium(II) complexes with AT sequences as compared to GC sequences are in good agreement with the experimental results. Interaction energy values suggest that the presence of a substituted aromatic ring in the intercalating ligand as well as the high surface area of intercalating and ancillary ligands increases the binding affinity of the metal complex towards DNA receptors. Hence, our computed results obtained from molecular docking and quantum mechanics/molecular mechanics calculations are very encouraging in the field of drug–DNA interaction.

Acknowledgements

Paritosh Mondal thanks the Department of Science and Technology (DST New Delhi, India) for financial support (SERB/F/1672/2013-14). Dharitri Das is thankful to the University Grants Commission (UGC), New Delhi, for providing non-net research fellowship.

References

1 A. Krishna, B. Kumar, B. M. Khan, S. K. Rawal and N. Krishna, *Biochim. Biophys. Acta*, 1998, **1381**, 104–112.
2 L. Nan, M. Ying, Y. Cheng, G. Liping and Y. Xiurong, *Biophys. Chem.*, 2005, **116**, 199–205.
3 A. M. Pizarro and P. J. Sadler, *Biochimie*, 2009, **91**, 1198–1211.
4 X. W. Liu, J. Li and H. Li, *J. Inorg. Biochem.*, 2005, **99**, 2372–2380.
5 E. Corral, C. G. A. Hotze and H. Den Dulk, *JBIC, J. Biol. Inorg. Chem.*, 2009, **14**, 439–448.
6 C. Metcalfe and J. A. Thomas, *Chem. Soc. Rev.*, 2003, **32**, 215–224.
7 P. U. Maheswari and M. Palaniandavar, *J. Inorg. Biochem.*, 2004, **98**, 219–223.
8 M. S. Deshpande, A. A. Kumbhar and A. S. Kumbhar, *Inorg. Chem.*, 2007, **46**, 5450–5452.
9 K. K. Ashwini, K. L. Reddy and S. Sirasani, *Supramol. Chem.*, 2010, **22**, 629–643.
10 K. L. Reddy, K. K. Ashwini and S. Sirasani, *Synth. React. Inorg., Met.-Org., Nano-Met. Chem.*, 2011, **41**, 182–192.
11 K. R. Sangeetha Gowda, B. B. Mathew, C. N. Sudhamani and H. S. B. Naik, *Biomed. Biotechnol.*, 2014, **2**, 1–9.

12 D. Tilala, H. Gohel, V. Dhinoja and D. Karia, *Int. J. ChemTech Res.*, 2013, **5**, 2329–2337.
13 J. K. Barton, K. E. Erkkila and D. T. Odom, *Chem. Rev.*, 1999, **99**, 2777–2796.
14 J. K. Barton, A. Danishefsky and J. M. Goldberg, *J. Am. Chem. Soc.*, 1984, **106**, 2172–2176.
15 M. Eriksson, M. Leijon, C. Hiort, B. Norden and B. Graeslund, *J. Am. Chem. Soc.*, 1992, **114**, 4933–4934.
16 L. S. Lerman, *J. Mol. Biol.*, 1961, **3**, 18–30.
17 A. E. Friedman, J. C. Chambron, J. P. Sauvage, N. J. Turro and J. K. Barton, *J. Am. Chem. Soc.*, 1990, **112**, 4960–4962.
18 Y. Jenkins, A. E. Friedman, N. J. Turro and J. K. Barton, *Biochemistry*, 1992, **31**, 10809–10816.
19 C. M. Dupureur and J. K. Barton, *J. Am. Chem. Soc.*, 1994, **116**, 10286–10287.
20 C. M. Dupureur and J. K. Barton, *Inorg. Chem.*, 1997, **36**, 33–34.
21 H. Song, J. T. Kaiser and J. K. Barton, *Nat. Chem.*, 2012, **4**, 615–620.
22 J. Andersson, L. H. Fornander, M. Abrahamsson, E. Tuite, P. Nordell and P. Lincoln, *Inorg. Chem.*, 2013, **52**, 1151–1159.
23 J. P. Hall, D. Cook, S. R. Morte, P. McIntyre, K. Buchner, H. Beer, D. J. Cardin, J. A. Brazier, G. Winter, J. M. Kelly and C. J. Cardin, *J. Am. Chem. Soc.*, 2013, **135**, 12652–12659.
24 K. E. Erkkila, D. T. Odom and J. K. Barton, *Chem. Rev.*, 1999, **99**, 2777–2795.
25 K. Maruyama, J. Motonaka, Y. Mishima, Y. Matsuzaki, I. Nakabayashi and Y. Nakabayashi, *Sens. Actuators, B*, 2001, **76**, 215–219.
26 J. Olofsson, L. M. Wilhelmsson and P. Lincoln, *J. Am. Chem. Soc.*, 2004, **126**, 15458–15465.
27 V. Rajendiran, M. Palaniandavar, V. S. Periasamy and M. A. Akbarsha, *J. Inorg. Biochem.*, 2012, **116**, 151–162.
28 V. S. Stafford, K. Suntharalingam, A. Shivalingam, A. J. P. White, D. J. Mann and R. Vilar, *Dalton Trans.*, 2014, DOI: 10.1039/c4dt02910k.
29 R. M. Hartshor and J. K. Barton, *J. Am. Chem. Soc.*, 1992, **114**, 5919–5925.
30 J. G. Vos and J. M. Kelly, *Dalton Trans.*, 2006, 4869–4883.
31 B. Elias and A. Kirsch-De Mesmaeker, *Coord. Chem. Rev.*, 2006, **250**, 1627–1641.
32 J. M. Kelly, A. B. Tossi, D. J. McConnell and C. A. O'hUigin, *Nucleic Acids Res.*, 1985, **13**, 6017–6034.
33 J. K. Barton, *Science*, 1986, **233**, 727–734.
34 A. Mukherjee, R. Lavery and B. Bagchi, *J. Am. Chem. Soc.*, 2008, **130**, 9747–9755.
35 F. Ahmadi, N. Jamali, R. Moradian and B. Astinchap, *DNA Cell Biol.*, 2012, **31**, 259–268.
36 F. Ahmadi, N. Jamali, S. Jahangard-Yekta, B. Jafari, S. Nouri, F. Najafi and M. Rahimi-Nasrabadi, *Spectrochim. Acta, Part A*, 2011, **79**, 1004–1012.
37 K. J. Morokuma, *Bull. Korean Chem. Soc.*, 2003, **24**, 797–801.
38 S. Dapprich, I. Komáromi, K. Suzie Byun, K. J. Morokuma and M. J. Frisch, *THEOCHEM*, 1999, **461–462**, 1–21.
39 T. Yoshida, Y. Munei, S. Hitaoka and H. Chuman, *J. Chem. Inf. Model.*, 2010, **50**, 850–860.
40 J. H. Alzate-Morales, J. Caballero, F. D. Gonzalez-Nilo and R. Contreras, *Chem. Phys. Lett.*, 2009, **479**, 149–155.
41 J. H. Alzate-Morales, J. Caballero, A. V. Jague and F. D. Gonzalez-Nilo, *J. Chem. Inf. Model.*, 2009, **49**, 886–899.
42 K. Gkionis, S. T. Mutter and J. A. Platts, *RSC Adv.*, 2013, **3**, 4066–4073.
43 Z. Futera and J. V. Burda, *J. Comput. Chem.*, 2014, **35**, 1446–1456.
44 Z. Futera, J. A. Platts and J. V. Burda, *J. Comput. Chem.*, 2012, **33**, 2092–20101.
45 D. Das, A. Dutta and P. Mondal, *RSC Adv.*, 2014, **4**, 60548–60556.
46 M. J. Frisch, G. W. Trucks, H. B. Schlegel, G. E. Scuseria, M. A. Robb, J. R. Cheeseman, G. Scalmani, V. Barone, B. Mennucci, G. A. Petersson, H. Nakatsuji, M. Caricato, X. Li, H. P. Hratchian, A. F. Izmaylov, J. Bloino, G. Zheng, J. L. Sonnenberg, M. Hada, M. Ehara, K. Toyota, R. Fukuda, J. Hasegawa, M. Ishida, T. Nakajima, Y. Honda, O. Kitao, H. Nakai, T. Vreven, J. A. Montgomery, J. E. Peralta, F. Ogliaro, M. Bearpark, J. J. Heyd, E. Brothers, K. N. Kudin, V. N. Staroverov, T. Keith, R. Kobayashi, J. Normand, K. Raghavachari, A. Rendell, J. C. Burant, S. S. Iyengar, J. Tomasi, M. Cossi, N. Rega, J. M. Millam, M. Klene, J. E. Knox, J. B. Cross, V. Bakken, C. Adamo, J. Jaramillo, R. Gomperts, R. E. Stratmann, O. Yazyev, A. J. Austin, R. Cammi, C. Pomelli, J. W. Ochterski, R. L. Martin, K. Morokuma, V. G. Zakrzewski, G. A. Voth, P. Salvador, J. J. Dannenberg, S. Dapprich, A. D. Daniels, O. Farkas, J. B. Foresman, J. V. Ortiz, J. Cioslowski and D. J. Fox, *Gaussian 09 (Revision B.01)*, Gaussian Inc., Wallingford, CT, 2010.
47 A. D. Becke, *Phys. Rev. A: At., Mol., Opt. Phys.*, 1988, **38**, 3098–3100.
48 C. Lee, W. Yang and R. G. Parr, *Phys. Rev.*, 1988, **37**, 785–789.
49 R. J. Nielsen, J. M. Keith, B. M. Stoltz and W. A. Goddard, *J. Am. Chem. Soc.*, 2004, **126**, 7967–7974.
50 P. J. Hay and W. R. Wadt, *J. Chem. Phys.*, 1985, **82**, 270–284.
51 P. C. Hariharan and J. A. Pople, *Chem. Phys. Lett.*, 1972, **16**, 217–219.
52 G. M. Morris, R. Huey, W. Lindstrom, M. F. Sanner, R. K. Below, D. S. Goodsell and A. J. Olson, *J. Comput. Chem.*, 2009, **30**, 2785–2791.
53 A. Robertazzi, A. Vittario Vargiu, A. Magistrato, P. Ruggerone, P. Carloni, P. D. Hoog and J. Reedijk, *J. Phys. Chem. B*, 2009, **113**, 10881–10890.
54 M. Svensson, S. Humbell, R. D. J. Froese, T. Matsubara, S. Sieber and K. Morokuma, *J. Phys. Chem.*, 1996, **100**, 19357.
55 T. Vresen and K. Morokuma, *J. Comput. Chem.*, 2001, **21**, 1419.
56 J. G. Liu, Q. L. Zhang, X. F. Shi and L. N. Ji, *Inorg. Chem.*, 2001, **40**, 5045–5050.
57 I. Fleming, *Frontier orbitals and organic chemical reactions*, Wiley, London, 1976.
58 J. I. Aihara, *J. Phys. Chem. A*, 1999, **103**, 7487–7495.
59 R. G. Pearson, *Hard and soft acids and bases*, Dowden, Hutchinson, Ross, Stroudsburg, PA, 1973.
60 R. G. Pearson, *J. Chem. Educ.*, 1987, **64**, 561–567.
61 R. Filosa, A. Peduto, S. Di Micco, P. de Caprariis, M. Festa, A. Petrella, G. Capranico and G. Bifulco, *Bioorg. Med. Chem.*, 2009, **17**, 13–24.
62 A. M. Pyle and J. K. Barton, *Prog. Inorg. Chem.*, 1990, **38**, 413–475.

RSC Advances

PAPER

View Article Online
View Journal | View Issue

Cite this: *RSC Adv.*, 2014, **4**, 60548

Interactions of the aquated forms of ruthenium(III) anticancer drugs with protein: a detailed molecular docking and QM/MM investigation

Dharitri Das, Abhijit Dutta and Paritosh Mondal*

Interaction of monoaqua and diaqua ruthenium complexes such as [*trans*-$RuCl_3(H_2O)$(3*H*-imidazole)(dmso-S)] **I**, [*trans*-$RuCl_2(H_2O)_2$(3*H*-imidazole)(dmso-S)]$^{+1}$ **II**, [*trans*-$RuCl_3(H_2O)$(4-amino-1,2,4-triazole)(dmso-S)] **III** and *trans*-$RuCl_2(H_2O)_2$(4-amino-1,2,4-triazole)(dmso-S)]$^{+1}$ **IV**, which are formed after intracellular aquation of their respective complexes, with human serum albumin (**HSA**) has been computationally investigated by molecular docking and two layer QM/MM hybrid methods. The computed binding energy of monoaqua adduct **I–HSA** and **III–HSA** evaluated by docking simulation are found to be −4.52 kcal mol^{-1} and −4.58 kcal mol^{-1} whereas the binding energy of diaqua adducts **II–HSA** and **IV–HSA** are evaluated to be −4.74 kcal mol^{-1} and −4.91 kcal mol^{-1}, respectively. Docking results also show that the ruthenium atoms of all the complexes are actively involved in coordination with histidyl nitrogen atoms in the active site of protein. In addition, in order to probe the stabilities of monoaqua and diaqua ruthenium complexes in the active site of protein, we have calculated their energetic by two layer QM/MM method. QM/MM study suggests higher stability of diaqua adduct, **II–HSA**. The stability of adducts varies in the order: **II–HSA** > **IV–HSA** > **I–HSA** > **III–HSA**. Binding energy values of all the complexes increase with the incorporation of solvent effect. Thus molecular docking and QM/MM results show that ruthenium complexes interact with the protein receptor more rapidly after their second hydrolysis. Hence, docking as well as ONIOM results will be highly beneficial for providing insight into the molecular mechanism of ruthenium complexes with protein receptor.

Received 17th September 2014
Accepted 31st October 2014

DOI: 10.1039/c4ra10630j

www.rsc.org/advances

Introduction

Platinum complexes like cisplatin, carboplatin, oxaliplatin *etc.* have been the most commonly used anticancer agents in chemotherapeutic treatment for the last thirty years. However, the high toxicity and undesirable side effects of these complexes[1,2] led to the discovery of new metal based anticancer agents.[3,4] Among the other metal complexes, ruthenium complexes are found to be effective alternatives to platinum.[5,6] Two Ru(III) complexes, NAMI-A and KP1019 are currently in phase II clinical trials.[7,8] NAMI-A has shown its activity against cancer metastases[9] while KP1019 is effective towards primary cancers.[10] Antimetastatic agents are extremely important in the treatment of cancer because 90 percent of cancer deaths are reported to be due to metastasis formation. NAMI-A complex is very unstable at physiological conditions like pH 7.4, [Cl] = 0.1 M, 37 °C. It has undergone hydrolysis after dissolution[11–14] and subsequent dissociation of chloride or DMSO ligand leading to the formation of diaqua derivatives.[12] It has been investigated further that dissociation process gives rise to formation of ruthenium complexes with only one imidazole and one chlorido ligands.[14] Hence to enhance hydrolytic stability, infusion solution of NAMI-A is dissolved in physiological concentration of sodium chloride, when given to patients.[15]

Over the past 25 years, a large number of studies have been carried out in order to clarify the mechanism of action of ruthenium complexes towards biomolecular target. In general, increasing evidences in the literature show that mechanism responsible for anticancer activities of ruthenium complexes are based on their DNA nucleobases interaction.[16–18] But before such interaction occurs, these complexes should be passed from cellular membrane to the nuclear membrane. During this time ruthenium complexes may interact with many active sites such as proteins, peptides and other molecular targets.[19–21] It is well-recognized that ruthenium complexes interact with protein receptor immediately after its intravenous administration.[22,23] Transferrin, which is mainly responsible for transporting iron to the body cells could be employed as a natural carrier for delivering cytotoxic ruthenium agents to tumor cells because of their higher demand for iron.[24,25] On the other hand albumin, a most abundant human plasma protein displays high binding affinity[26] and act as a reservoir for the transferrin cycle. Lots of efforts have been devoted for investigating the interactions between ruthenium complexes and proteins. It is believed that ruthenium complexes tend to coordinate N-side chains of

Department of Chemistry, Assam University, Silchar 788011, Assam, India. E-mail: paritos_au@yahoo.co.in

amino acids like histidine, arginine as well as other amino acids, since these complexes are known to bind selectively to imine sites in biomolecules.[27,28] Also there are evidences for binding of ruthenium to sulfur (S donor/thiolate) compounds, but these complexes are kinetically unstable, especially in the presence of oxygen.[29,30] The interactions are generally facilitated by aqua derivatives of ruthenium(III) complexes because these derivatives are much more reactive towards intracellular target as compared to their parent chloro complexes. In case of NAMI-A, very interesting information have been obtained when crystal structures of lactoferrin–NAMI-A[31] and carbonic anhydrase–NAMI-A adducts[32] are examined. The crystal structure of carbonic anhydrase–NAMI-A adduct reveals that ligands of ruthenium complex are progressively lost during protein binding and in final adduct ruthenium complex retains its octahedral arrangement completed by water molecules, imidazolium nitrogen atom of His64 and carbonyl oxygen atom of Asn62.[32] Recently, Vergara *et al.*[33] has investigated the binding properties of a new NAMI-A analogue called azi-Ru, which is more cytotoxic and shows higher antiproliferative activity than NAMI-A towards hen egg lysozyme (HEWL). They have reported that azi-Ru binds with the protein lysozyme through His15 and Asp87 amino acid residue. So far, numbers of experimental researches on mode of action of ruthenium-based drugs (including the hydrolysis mechanism and binding to biomolecules) have been done but to the best of our knowledge only a few computational studies have been performed at the molecular level.[34] Besker *et.al.*[35] have published a DFT study on binding nature of antitumor ruthenium(II) and ruthenium(III) complexes with DNA and protein. It is found that N7 of guanine, histidyl imidazole residue and sulfur containing methionine and cysteine residues are the preferred binding sites for ruthenium complexes. Chen *et al.*[36] has investigated the two step hydrolysis reaction of NAMI-A by DFT method where they found that chloroaquated and *cis* diaquated species of NAMI-A is thermodynamically more stable than corresponding *trans* diaquated species. Recently, many studies have reported the stepwise mechanism of interaction of monoaquated and diaquated species of metal complexes with DNA and protein residues.[37–39]

Present work examines the stability and binding affinity of monoaqua and diaqua complexes of NAMI-A: [*trans*-$RuCl_3(H_2O)$-(3*H*-imidazole)(dmso-S)] (**I**), [*trans*-$RuCl_2(H_2O)_2$(3*H*-imidazole)(dmso-S)]$^{+1}$ (**II**) and its amino derivative: [*trans*-$RuCl_3(H_2O)$(4-amino-1,2,4-triazole)(dmso-S)] (**III**) and *trans*-$RuCl_2(H_2O)_2$(4-amino-1,2,4-triazole)(dmso-S)]$^{+1}$ (**IV**) with human serum albumin (**HSA**). Currently, it is not clear whether monoaqua or diaqua complexes or both of them are active species before reaction with protein receptor. Therefore we have considered both monoaqua and diaqua form of ruthenium(III) complexes for protein interaction. In order to find out the stability and binding affinity of anticancer drugs with protein receptor, many researchers have utilized two powerful computational strategies: docking and ONIOM (Our own N-layered Integrated molecular Orbital and Molecular Mechanics).[40–42] In the current study, to find out the appropriate orientation of the metal complex into the binding site of protein receptor, molecular docking simulations are taken up in an initial step and then quantum chemical calculations are performed using two layer ONIOM method.

Computational details

Structure

DFT optimized geometry of **I**, **II**, **III** and **IV** complexes in gas phase are obtained using unrestricted Becke's[43] three parameter hybrid exchange functional (B3) and the Lee–Yang–Parr correlation functional (LYP) (B3LYP)[44] functional with LANL2DZ + 6-31G (d,p) basis sets. LANL2DZ basis set[45] which describe effective core potential of Wadt and Hay (Los Alamos ECP) on ruthenium atom and 6-31G (d,p) basis set[46] for all other non metal atoms are used for ground state geometry optimization. LANL2DZ basis set is used as it reduces the calculation time containing larger nuclei. Vibrational analysis has been performed at the same level of theory for achieving energy minimum. GAUSSIAN 09 program package[47] is employed to carry out all the DFT calculations.

Molecular docking simulation

DFT optimized structure of ruthenium complexes such as **I**, **II**, **III** and **IV** and crystal structure of human serum albumin (**HSA**) entitled 1H9Z, obtained from research collaboratory for structural bioinformatics (RCSB) protein data bank are taken for molecular docking simulation. The three homologous domains of **HSA** are 1, 2, 3 each of which is composed of A and B subdomains.[48] Site 1 and site 2, located in hydrophobic cavities in subdomains 2A and 3A are the two major drug binding site of **HSA**.[48,49] Some recent investigations have demonstrated that anthracycline drugs bind to a non classical binding site on subdomain 1B of **HSA**.[50,51] Therefore in this study, subdomain 1B has been chosen as ligand binding site during docking simulation. Autodock 4.2 program,[52] an interactive molecular graphics program is used to perform molecular docking simulation. For docking, the protein structure in pdb format is prepared by structure preparation tool available in Auto Dock Tools package version 1.5.4. All the water molecules and the residues (warfarin moieties namely coumarin, benzyl and acetonyl which are found to be complexed with **HSA** receptor) have been removed from the crystal structure of **HSA** and then polar hydrogen atoms are added for saturation, Gasteiger charges are computed and non-polar hydrogen atoms are merged. A grid box with grid spacing of 0.375 Å and dimension of $60 \times 60 \times 60$ grid points along x, y and z axes are built around the ligand binding site. The grid box carries the complete binding site of the protein receptor and gives sufficient space for the ligand translational and rotational walk. Finally, ten possible docking runs are performed with step sizes of 2 Å for translation and 50° for rotation. A maximum number of energy evaluations are set to 25 000 and a maximum number of 27 000 GA operations are generated with an initial population of 150 individuals. The rate of gene mutation and crossover are set to 0.02 and 0.80, respectively.

QM/MM calculation

The lowest energy structure, obtained from preceding docking simulation is chosen as the starting geometry for the two layer ONIOM study. The residues located outside the active site region of protein receptor are removed in order to reduce the system size. Investigation of the whole protein–ligand adduct by quantum mechanics (QM) is very computationally demanding. Hence, we have applied QM on the interacting residues with the ruthenium complex and molecular mechanics (MM) for the remaining part of the system (Fig. 1). For monoaquated adduct, the QM region is composed of ruthenium complex, His146 and Gln459 residue while MM region is composed of Ala194, Arg145, Arg197, Asp108, Glu425, Leu463, Phe149, Pro147, Ser193 and Tyr148 residue respectively. Here charge of both the layer is set to be 0. On the other hand, for diaquated adducts, QM part includes ruthenium complex, His146 and Ser193. Along with these two residues Lys190 (for **II–HSA**), Pro147 and Glu425 (for **IV–HSA**) are included in the QM layer. The charge of QM set for diaquated adduct is set to be +1. Finally, the whole structure is optimized using two layer ONIOM method by treating QM region at UB3LYP/(LANL2DZ + 6-31G (d,p)) level. MM region is described using universal force field, implemented in GAUSSIAN 09 program. In the two layers ONIOM method, the total energy (E_{ONIOM}) of the entire system is obtained from three independent energy calculations:

$$E^{ONIOM2} = E^{high}_{model\ system} + E^{low}_{real\ system} - E^{low}_{model\ system}$$

Real system contains full geometry of the molecule and is considered as MM layer while the model system contains the chemically most important (core) part of the system that is considered as QM layer.

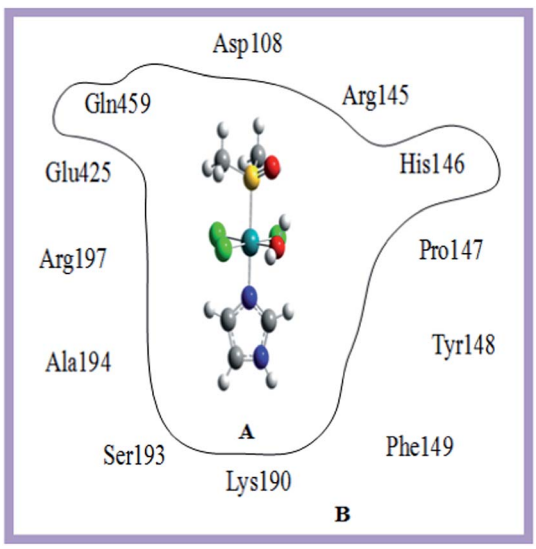

Fig. 1 Schematic 2D diagram of the model system for ruthenium complex bound to HSA binding site. Layers that are partitioned are shown for ONIOM2 calculations. A is the inner layer (QM calculations) and B is the outer layer (MM calculations). The arrangement of the residues shown in 2D diagram is not their actual position in 3D.

To find the relative stability of respective adducts, we have evaluated the interaction energy, ΔE, which is given by the expression:

$$\Delta E = \Delta E_{HSA/Ru-complex} - \Delta E_{HSA} - \Delta E_{Ru-complex}$$

$\Delta E_{HSA/Ru-complex}$ is the energy of the optimized adduct of complex–**HSA**, ΔE_{HSA} is the energy of the optimized **HSA** receptor and the $\Delta E_{Ru-complex}$ is the energy of the optimized ruthenium complexes.

To observe effect of solvation in the ruthenium complex–**HSA** interaction, single-point calculations have been performed on the interacting part of the protein by the UB3LYP functional, using LANL2DZ and 6-31G (d,p) basis sets and conductor-like polarized continuum model.[53,54] In order to reduce the calculation time, we have taken only the high level (QM) part for single point calculation.

Results and discussion

Structural analysis of monoaqua and diaqua complexes

Important geometrical parameters of the ruthenium complexes evaluated in gas phase are presented in Table 1 and their optimized geometries evaluated by DFT at B3LYP level are shown in Fig. 2. In complex **I**, the Ru–Cl_1, Ru–Cl_2, Ru–Cl_3, Ru–O, Ru–N and Ru–S bond lengths are calculated to be 2.43 Å, 2.38 Å, 2.34 Å, 2.21 Å, 2.10 Å and 2.36 Å respectively. Ru–O bond length is found to be shorter than that of Ru–Cl bond lengths, indicating the stronger coordination ability of water ligands than that of chloride ligands. The coordinated water molecule of complex **I** form a hydrogen bond with DMSO oxygen atom (1.85 Å). The bond angles Cl_1–Ru–O(wat1), O(wat1)–Ru–Cl_2, Cl_2–Ru–Cl_3 and Cl_3–Ru–Cl_1 of the complex **I** are found to be as: 80.6°, 86.3°, 97.2° and 95.7°, respectively. As a consequence of this deviation of bond angles from 90°, the geometry about the ruthenium atom is distorted from regular octahedral structure.

Table 1 Selected bond lengths (Å) and bond angles (°) calculated for ruthenium(III) complexes at B3LYP level in the gas phase

Parameters	I	II	III	IV
Ru–Cl_1	2.43	2.34	2.41	2.32
Ru–Cl_2	2.38		2.41	
Ru–Cl_3	2.34	2.31	2.33	2.30
Ru–O(wat1)	2.21	2.23	2.24	2.24
Ru–O(wat2)		2.16		2.18
Ru–N_1	2.10	2.10	2.10	2.09
Ru–S_1	2.36	2.41	2.36	2.41
N_1–Ru–S_1	176.3		176.1	175.5
Cl_1–Ru–Cl_2	167.1		165.5	
Cl_1–Ru–O(wat1)	80.6	83.9	85.1	85.6
O(wat1)–Ru–Cl_2	86.3		80.5	
O(wat1)–Ru–O(wat2)		85.5		82.5
O(wat2)–Ru–Cl_3		91.2		90.1
Cl_2–Ru–Cl_3	97.2		97.6	
Cl_3–Ru–Cl_1	95.7	99.8	96.9	99.9

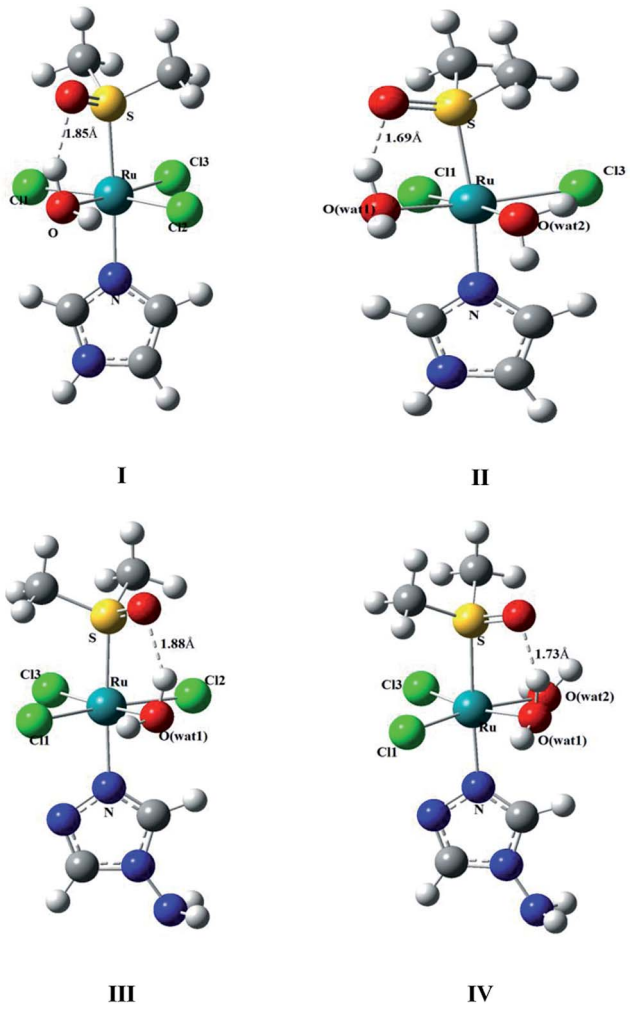

Fig. 2 Optimized geometries of ruthenium(III) complexes with appropriate numbering obtained from B3LYP/(LanL2DZ + 6-31G**) calculation.

For complex **II**, ruthenium atom is coordinated with two water molecules and one of the two water molecules have formed hydrogen bonding interaction with DMSO oxygen atom within a distance of 1.70 Å. Ru–O(wat1) and Ru–O(wat2) bond lengths are found to be 2.23 and 2.16 Å, respectively. Complex **II** also exhibits pseudooctahedral configuration having Cl_1–Ru–O(wat1), O(wat1)–Ru–O(wat2), $(wat2)_2$–Ru–Cl_3 and Cl_3–Ru–Cl_1 bond angles are in the range of 83.9°–99.8°. These geometrical parameters are comparable with available experimental data. Similar geometrical parameters are also reported by Chen *et al.* on studying the aquation of NAMI-A.[36] However, slightly higher values of bond lengths of all complexes are thought to be due to systematic errors caused by computation method, basis set and environment factors.[36] Electronic structures of complex **III** and complex **IV** are found to be similar to that of complex **I** and complex **II**.

Stability of the ruthenium complexes

Chemical properties of ruthenium complexes are determined by analyzing the nature of highest occupied molecular orbital (HOMO) and the lowest unoccupied molecular orbital (LUMO). Calculated LUMO and HOMO energies of the ruthenium complexes are listed in Table 2. With the help of LUMO–HOMO energy separation, the kinetic stability and relative reactivity pattern of a chemical system can be predicted. The lower value of energy separation indicates higher reactivity and lower kinetic stability of a molecule.[55] Pearson pointed out that the LUMO–HOMO energy separation represents the chemical hardness which is a reliable reactivity parameter to predict the stability of a molecule.[56] Greater stability of molecules is due to their higher hardness value as stated by maximum hardness principle.[57] It is observed from computational investigation that complex **II** (Table 2) having higher value of LUMO–HOMO energy gap as well as higher chemical hardness value, exhibits higher stability than that of complex **I**, **III** and **IV**.

Table 2 Energies of HOMO (E_H in eV) and LUMO (E_L in eV) and chemical hardness (η in eV) of ruthenium(III) complexes

Complex	E_H	E_L	ΔE	η
I	−6.204	−3.646	2.558	1.279
II	−10.095	−7.335	2.758	1.379
III	−6.177	−3.646	2.531	1.266
IV	−9.905	−7.510	2.395	1.198

Docking study

The analysis of molecular docking calculations between ruthenium complexes with **HSA** shows that all the complexes exhibit almost similar binding orientation. The interaction energy of all the protein adducts along with their experimental binding constant (metal complexes binding to albumin)[58] are reported in Table 3. The binding energy for **I–HSA**, **II–HSA**, **III–HSA** and **IV–HSA** adducts are evaluated to be −4.52, −4.74, −4.58 and −4.91 kcal mol^{-1}. The larger negative value of binding energy reflects greater binding affinity of ruthenium complexes with the protein receptor. The most important amino acid components involved in binding interaction with protein receptor are Ala194, Arg145, Arg197, Asp108, Gln459, Glu425, His146, Lys190, Phe149, Pro147 and Tyr148. Docking results of ruthenium complexes are shown in Fig. 3 and 4 and possible binding interaction of ruthenium complexes with the receptor in terms of hydrogen bond and metal–receptor interaction are presented in Table 4. Fig. 3 shows the binding interaction of **I** and **III** at the surface binding site of subdomain 1B. Complex **I** form a hydrogen bonding interaction with the amino acid residue Gln459 at a distance of about 1.90 Å through its DMSO oxygen

Table 3 Binding energy (ΔE in kcal mol^{-1}) and binding constant (k_b in min^{-1}) of all the complexes with HSA, evaluated by molecular docking

Adducts	ΔE	k_b (experimental data)
I–HSA	−4.52	0.210
II–HSA	−4.74	
III–HSA	−4.58	0.436
IV–HSA	−4.91	

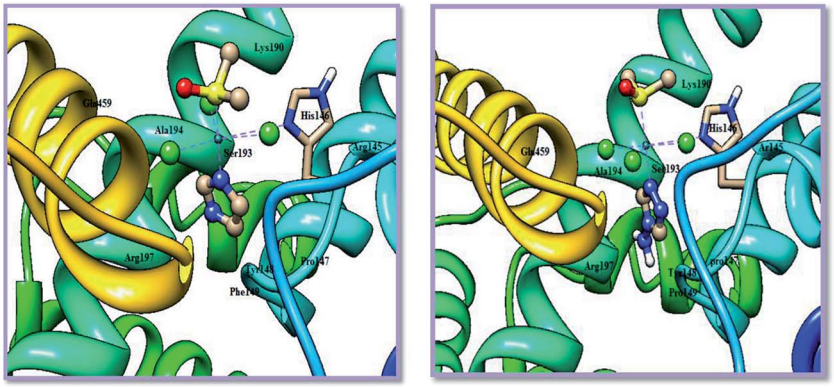

Fig. 3 Docked structures of monoaquated adducts at the active site of protein receptor. The rest part of protein structure is not shown for clarity.

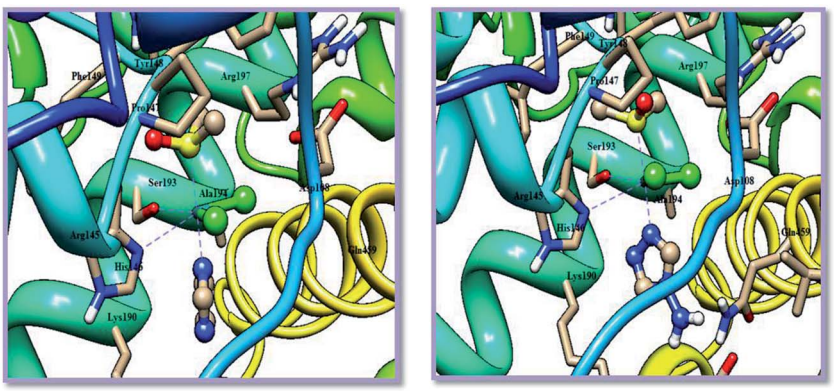

Fig. 4 Docked structures of diaquated adducts at the active site of protein receptor. The rest part of protein structure is not shown for clarity.

Table 4 Hydrogen bond and metal–receptor interaction of ruthenium(III) complexes with HSA evaluated by docking analysis

		Amino acid residue involved in hydrogen bonding
		HSA
Adducts	Groups	Amino acid residue
I–HSA	DMSO O atom	*H*NGln459 (1.90 Å)
	Metal–receptor	*N*-imidazole His146 (3.00 Å)
II–HSA	DMSO O atom	*H*CH_2His146 (1.69 Å)
	Imidazolium H atom	*O* Lys190 (2.79 Å)
	Metal–receptor	*N*-imidazole His146 (3.05 Å)
	Metal–receptor	*O*Ser193 (2.15 Å)
III–HSA	DMSO O atom	*H*NGln459 (1.93 Å)
	Metal–receptor	*N*-imidazole His146 (4.05 Å)
IV–HSA	Metal–receptor	*N*-imidazole His146 (3.03 Å)
	Metal–receptor	*O*Ser193 (2.57 Å)
	Imidazole H atom	*O* Glu425 (2.32 Å)

atom and a metal receptor interaction is observed with the His146 residue at a distance of about 3.00 Å. A similar orientation is observed for docked structure of complex **III** as it shows a hydrogen bonding interaction with the amino acid residue Gln459 (1.93 Å) and a metal receptor interaction with the residue His146 (4.05 Å). Fig. 4 presents the docked structure of complex **II** and complex **IV** at the active site of the protein receptor. Two hydrogen bonding interaction of the complex **II** with amino acid residue His146 (1.69 Å) and Lys190 (2.79 Å) have been observed through its DMSO oxygen atom and imidazolium hydrogen atom while only a single hydrogen bonding interaction is observed for complex **IV** with Glu425 residue at a distance of 2.32 Å. Both the complexes form metal receptor interaction with His146 and Ser193 within a distance of 3.05 Å. As it is observed, the interaction between ruthenium complexes and **HSA** is not completely hydrophobic in nature since there are several ionic (Asp108, Glu425, Arg145, Arg197 and Lys190) and polar residues (His146, Ser193, Tyr148 and Gln459) in the proximity of the bound ligand (within 4 Å) playing crucial role in stabilizing ruthenium complexes *via* hydrogen bonding and electrostatic interactions.

ONIOM study

Structural characteristics

The fully optimized structures of all the adducts of ruthenium complexes with **HSA** calculated at UB3LYP/6-31G (d,p): UFF level are shown in Fig. 5 and significant geometrical parameters are listed in Table 5.

Monoaqua interaction

From Fig. 5 and Table 5, it is seen that inside the binding site of **HSA**, complex **I** has retained its pseudooctahedral configuration, in which water ligand has been replaced from the system by histidyl residue and coordinated with the ruthenium atom at a distance ($Ru–N_{His}$) of 2.18 Å. The Ru–Cl bond lengths are in the range of 2.38–2.42 Å whereas Ru–N and Ru–S bond lengths are 2.11 and 2.43 Å, respectively. It is also observed that complex **I** forms a hydrogen bond between DMSO oxygen atom and one of the hydrogen atoms of glutamine side chain. The existence of the hydrogen bonding in this adduct is indicated by the two important aspects: (i) short $DMSO–H_{Gln}$, contact distance of 2.03 Å (ii) deviations of $Cl_1–Ru–N_{His}$ (85.7°) and $Cl_2–Ru–N_{His}$ (88.1°) bond angle from the octahedral 90° value. Presences of hydrogen bonding gives additional stability to this adduct. The calculation shows that the dihedral angle $Cl_3–Cl_2–N_{His}–C$ of **I–HSA** is 91.5° which indicate that histidyl ring is found to be perpendicular to the molecular plane about its central axis. Electronic structures of **I–HSA** and **III–HSA** are found to be similar but $Ru–N_{His}$ bond is slightly longer in **III–HSA**, indicating a weaker coordination ability of complex **III** as compared to complex **I**. The dihedral angle $Cl_3–Cl_2–N_{His}–C$ of **III–HSA** is found to be 47.6° reflecting a deviation of histidyl ring from molecular plane.

Diaqua interaction

In **II–HSA**, the ruthenium atom is coordinated with histidyl nitrogen atom and oxygen atom of serine residue of protein receptor at a distance of 2.18 and 1.89 Å. The angle $Cl_1–Ru–N_{His}$ is 84.1° whereas the angle $O_{Ser}–Ru–N_{His}$ is 88.8°. This observed deviation of bond angles from 90° clearly indicates a distortion of geometry from regular octahedral structure. Complex **II** form two intermolecular hydrogen bonding with the protein receptor: DMS*O*–H_{His} at 2.06 Å and imidazoliumC*H*–O_{Lys} at 2.28 Å. The geometrical parameters of **II–HSA** and **IV–HSA** are almost similar but the latter one is stabilized by presence of two additional hydrogen bonding with glutamic acid residue *via* imidazolium hydrogen atom. The dihedral angle ($Cl_3–O–N_{His}–C$) of **II–HSA** is found to be 116.7° and for **IV–HSA** is 94.7°.

Stability

In order to find out the stability of the four adducts we have evaluated the binding energy which are presented in Table 6 along with the absolute energy values of the interacting moieties. These results shown in Table 6 allow us to conclude that

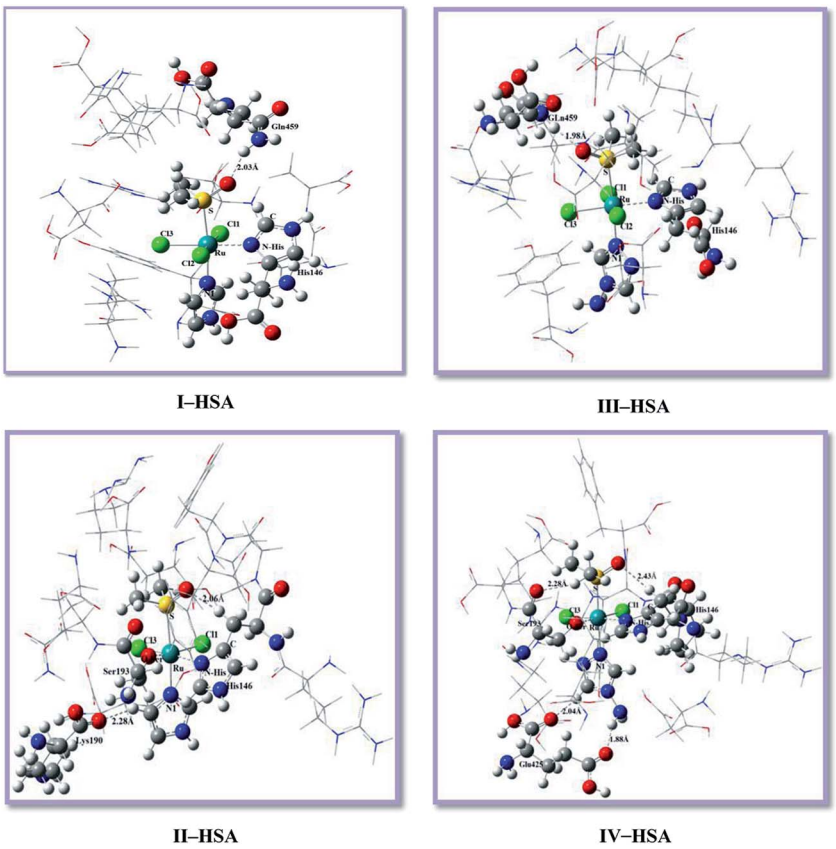

Fig. 5 Optimized geometries of monoaquated and diaquated adducts with appropriate numbering obtained from two layer QM/MM method.

Table 5 Calculated bond length (Å) and bond angles (°) of monoaquated and diaquated adduct

	I–HSA		**III–HSA**		**II–HSA**		**IV–HSA**	
	Ru-coordination	Hydrogen bonding	Ru-coordination	Hydrogen Bonding	Ru-coordination	Hydrogen bonding	Ru-coordination	Hydrogen bonding
Ru–N_{His}	2.18		2.25		2.18		2.16	
Ru–O_{Ser}					1.89		1.99	
Ru–Cl_1	2.42		2.45		2.38		2.38	
Ru–Cl_2	2.40		2.38					
Ru–Cl_3	2.38		2.36		2.34		2.47	
Ru–S	2.43		2.42		2.48		2.37	
Ru–N	2.11		2.10		2.14		2.16	
DMS*O*–H_{Gln}		2.03		1.98				
DMS*O*–H_{His}						2.06		2.43
Imidazolium*CH*–O_{Lys}						2.28		
DMSOCH_2*H*–O_{Ser}						2.50		2.28
Imidazolium*NH*–O_{Glu}								1.88
Imidazolium*CH*–O_{Glu}								2.04
Cl_1–Ru–N_{His}	85.7		87.2		84.1		94.9	
Cl_2–Ru–N_{His}	88.1		93.5					
Cl_2–Ru–Cl_3	92.8		91.5					
Cl_3–Ru–Cl_1	93.4		87.8		92.6		85.2	
O_{Ser}–Ru–N_{His}					88.8		87.8	
O_{Ser}–Ru–Cl_3					95.5		92.1	
Cl_3–Cl_2–N_{His}–C	91.5		47.6					
Cl_3–O–N_{His}–C					116.7		94.7	

Table 6 Absolute energy values (in au) of interacting adducts and calculated binding energy ($\Delta E \times 10^2$ in kcal mol^{-1}) of ruthenium complexes with HSA calculated by two layer ONIOM method in gas phase. Interacting part of HSA in aqueous phase is calculated by high level UB3LYP/(LANL2DZ + 6-31G (d,p)) method

	Gas phase				Solvent phase			
Adduct	$\Delta E_{HSA/Ru-complex}$	ΔE_{HSA}	$\Delta E_{Ru-complex}$	ΔE	$\Delta E_{HSA/Ru-complex}$	ΔE_{HSA}	$\Delta E_{Ru-complex}$	ΔE
I–HSA	−3333.57	−1080.52	−2330.49	479.67	−3334.66	−1080.58	−2330.52	479.70
II–HSA	−3087.34	−1293.53	−1946.47	958.50	−3087.34	−1293.65	−1946.56	959.23
III–HSA	−3405.91	−1080.52	−2401.83	479.62	−3405.99	−1080.58	−2401.86	479.69
IV–HSA	−3538.64	−1672.88	−2017.81	954.12	−3538.68	−1672.92	−2017.98	954.68

the binding energies of diaqua adducts are higher than that of monoaqua adducts. That is diaqua adducts are more stable than the corresponding monoaqua adducts. Again, **IV–HSA** have lowest absolute energy value ($\Delta E_{HSA/Ru-complex}$), suggesting that this diaqua form of amino derivative of NAMI-A has higher reactivity towards protein receptor, in agreement with the experimental studies reported by Grossl *et al.*[58] This is mainly due to the presence of primary amine group in this derivative which favors formation of hydrogen bonding interaction towards protein residues, making protein–complex conjugation. In spite of its higher reactivity towards protein receptor, the evaluated binding energy of **IV–HSA** adduct is lower as compared to **II–HSA** and hence exhibited less stability than that of **II–HSA**. **II–HSA** having energy 958.50 × 10^2 kcal mol^{-1} being the most stable adduct followed by **IV–HSA, I–HSA** and **III–HSA.**

Since all biological interactions are occur in aqueous environments, we have carried out single point calculations on interacting part of all the four adducts to get an estimate of the solvent effect. Inclusion of solvent effect in energy calculations lead to changes in energy and stability of the corresponding adducts. The order of binding energy in aqueous solution is found to be in the order: **II–HSA** > **IV–HSA** > **I–HSA** > **III–HSA.** The binding energies of all adducts are evaluated to be higher compared to their respective counterpart in gas phase, indicating the increased stability of all the adducts with the inclusion of solvent medium.

Conclusion

Molecular docking and QM/MM calculation has been carried out for monoaqua and diaqua ruthenium(III) complexes in order to evaluate the binding affinity and stability of the complexes in protein environment. Molecular docking simulation shows that diaqua adduct *i.e.* **II–HSA** and **IV–HSA** has exhibited higher binding affinity than the corresponding monoaqua adducts (**I–HSA** and **III–HSA**). These studies reveal that in the active site of

protein, residues Ala194, Arg145, Arg197, Asp108, Gln459, Glu425, His146, Lys190, Phe149, Pro147 and Tyr148 play a key role in binding with the complexes. In monoaqua adducts, ruthenium complex are found to interact with His146 and Gln459 while ruthenium complexes in diaqua adducts interact with Ser193, Lys190 and Glu425 in addition to His146. Again, two layer ONIOM calculations analyze the stability and energetic details of the interacting ruthenium complexes with protein. The binding energy evaluated by ONIOM calculation suggests the highest stability of **II–HSA** adduct. However, interaction energy of **IV–HSA** adduct is higher than other adduct indicating higher reactivity of complex **IV** towards protein, in agreement with experimental data. Binding energy values suggest that diaqua adducts is more stable than monoaqua adducts. Presence of more hydrogen bonding in diaqua adducts gives extra stability as compared to monoaqua adducts. In addition, the interaction energies of all the four adduct increases in water solvent.

Acknowledgements

Author Paritosh Mondal thanks Department of Science and Technology (DST), New Delhi, India for financial support (SR/FT/CS-86/2010). Dharitri Das is thankful to the University Grants Commission (UGC), New Delhi for providing research fellowship. Abhijit Dutta is thankful to the DST – SERB project, New Delhi for providing research fellowship.

References

1 V. Bravec and J. Kasparkova, *Drug Resist. Updates*, 2005, **8**, 131–146.
2 I. Kostova, *Curr. Med. Chem.*, 2006, **13**, 1085–1107.
3 D.-L. Ma, L.-J. Liu, K.-H. Leung, Y.-T. Chen, H.-J. Zhong, D. S.-H. Chan, H.-M. D. Wang and C.-H. Leung, *Angew. Chem., Int. Ed.*, 2014, **53**, 1–6.
4 H.-J. Zhong, K.-H. Leung, L.-J. Liu, L. Lu, D. S.-H. Chan, C.-H. Leung and D.-L. Ma, *ChemPlusChem*, 2014, **79**, 508–511.
5 M. A. Jakupec, M. Galanski and B. K. Keppler, *Rev. Physiol., Biochem. Pharmacol.*, 2003, **146**, 1–54.
6 Z. Travnicek, M. Matikova-Malarova, R. Novotna, J. Vanco, K. Stepankova and P. Suchy, *J. Inorg. Biochem.*, 2011, **105**, 937–948.
7 T. Pieper, K. Borsky and B. K. Keppler, *Top. Biol. Inorg. Chem.*, 1999, **1**, 171–199.
8 G. Sava, E. Alessio, A. Bergamo and G. Mestroni, *Top. Biol. Inorg. Chem.*, 1999, **1**, 143–169.
9 M. Bouma, B. Nuijen, M. T. Jansen, G. Sava, A. Flaibani, S. Bult and J. H. Beijen, *J. Pharm. Biomed. Anal.*, 2002, **30**, 1287–1296.
10 J. Reedijk, *Curr. Opin. Chem. Biol.*, 1999, **3**, 236–240.
11 M. Bacac, A. C. G. Hotze, K. van der Schilden, J. G. Haasnoot, S. Pacor, E. Alessio, G. Sava and J. Reedijk, *J. Inorg. Biochem.*, 2004, **98**, 402–412.
12 M. Brindell, I. Stawoska, J. Supel, A. Skoczowski, G. Stochel and R. van Eldik, *J. Biol. Inorg. Chem.*, 2008, **13**, 909–918.
13 M. Bouma, B. Nuijen, M. T. Jansen, G. Sava, A. Flaibani, A. Bult and J. H. Beijnen, *Int. J. Pharm.*, 2002, **248**, 239–246.
14 M. Webb and C. Walsby, *Dalton Trans.*, 2011, **40**, 1322–1331.
15 M. Groessl, C. G. Hartinger, P. J. Dyson and B. K. Keppler, *J. Inorg. Biochem.*, 2008, **102**, 1060–1065.
16 V. Brabec and O. Novakova, *Drug Resist. Updates*, 2006, **9**, 111–122.
17 O. Novakova, J. Kasparkova, O. Vrana, P. M. Van Vliet, J. Reedijk and V. Brabec, *Biochemistry*, 1995, **34**, 12369–12378.
18 C. G. Kuehn and H. Taube, *J. Am. Chem. Soc.*, 1976, **98**, 689; S. Fruhauf and W. Zeller, *Cancer Res.*, 1991, **51**, 2943–2948.
19 K. Hindmarsh, D. A. House and M. M. Turnbull, *Inorg. Chim. Acta*, 1997, **257**, 11–18.
20 L. G. Marzilli, S. O. Ano, F. P. Intini and G. Natile, *J. Am. Chem. Soc.*, 1999, **121**, 9133–9142.
21 J. Arpalahti, M. Mikola and S. Mauristo, *Inorg. Chem.*, 1993, **32**, 3327–3332.
22 L. Messori, F. Gonzales Vilchez, R. Vilaplana, F. Piccioli, E. Alessio and B. K. Keppler, *Met.-Based Drugs*, 2000, **7**, 335–342.
23 F. Piccioli, S. Sabatini, L. Messori, P. Orioli, C. G. Hartinger and B. K. Keppler, *J. Inorg. Biochem.*, 2004, **98**, 1135–1142.
24 P. T. Gomme, K. B. McCann and K. B. Bertolini, *Drug Discovery Today*, 2005, **10**, 267–273.
25 E. Reisner, V. B. Arion, C. G. Hartinger, M. A. Jakupec, A. J. L. Pombeiro and B. K. Keppler, in *Education in Advanced Chemistry*, ed. A. M. Trzeciak, Wydawnictwo Uniwersytetu Wroctawskiego, n-Wrocław, 2005, vol. 9, pp. 215–229.
26 K. Polec-Pawlak, J. K. Abramski, O. Semenova, C. G. Hartinger, A. R. Timerbaev, B. K. Keppler and M. Jarosz, *Electrophoresis*, 2006, **27**, 1128–1135.
27 M. J. Clarke, F. Zu and D. R. Frasca, *Chem. Rev.*, 1999, **99**, 2511–2533.
28 M. J. Clarke, *Coord. Chem. Rev.*, 2002, **232**, 69–93.
29 D. Frasca and M. J. Clarke, *J. Am. Chem. Soc.*, 1999, **121**, 8523–8532.
30 M. Zhao and M. J. Clarke, *J. Biol. Inorg. Chem.*, 1999, **4**, 318–340.
31 C. A. Smith, A. J. Sutherland-Smith, B. K. Keppler, F. Kratz and E. N. Baker, *J. Biol. Inorg. Chem.*, 1996, **1**, 424–431.
32 A. Casini, C. Temperini, C. Gabbiani, C. T. Supuran and L. Messori, *ChemMedChem*, 2010, **3**, 1989–1994.
33 A. Vergara, G. D'Errico, D. Montesarchio, G. Mangiapia, L. Paduan and A. Merlino, *Inorg. Chem.*, 2013, **52**, 4157–4159.
34 J.-C. Chen, L.-M. Chen, L.-C. Xu, K.-C. Zheng and L.-N. Ji, *J. Phys. Chem. B*, 2008, **112**, 9966–9974.
35 N. Besker, C. Coletti, A. Marrone and N. Re, *J. Phys. Chem. B*, 2007, **111**, 9955–9964.
36 J. Chen, L. Chen, S. Liao, K. Zheng and L. Ji, *J. Phys. Chem. B*, 2007, **111**, 7862–7869.
37 S. Banerjee and A. K. Mukherjee, *Inorg. Chim. Acta*, 2013, **400**, 130–141.
38 Q. Fu, L. Zhou and J. Li, *Struct. Chem.*, 2012, **23**, 1931–1940.
39 P. Sarmah and R. C. Deka, *J. Mol. Struct.: THEOCHEM*, 2010, **955**, 53–60.

40 T. Yoshida, Y. Munei, S. Hitaoka and H. Chuman, *J. Chem. Inf. Model.*, 2010, **50**, 850–860.
41 J. H. Alzate-Morales, J. Caballero, F. D. Gonzalez-Nilo and R. Contreras, *Chem. Phys. Lett.*, 2009, **479**, 149–155.
42 J. H. Alzate-Morales, J. Caballero, A. V. Jague and F. D. Gonzalez-Nilo, *J. Chem. Inf. Model.*, 2009, **49**, 886–899.
43 A. D. Becke, *Phys. Rev. A*, 1988, **38**, 3098–3100.
44 C. Lee, W. Yang and R. G. Parr, *Phys. Rev.*, 1988, **37**, 785–789.
45 P. J. Hay and W. R. Wadt, *J. Chem. Phys.*, 1985, **82**, 270–284.
46 P. C. Hariharan and J. A. Pople, *Chem. Phys. Lett.*, 1972, **16**, 217–219.
47 M. J. Frisch, G. W. Trucks, H. B. Schlegel, G. E. Scuseria, M. A. Robb, J. R. Cheeseman, G. Scalmani, V. Barone, B. Mennucci, G. A. Petersson, H. Nakatsuji, M. Caricato, X. Li, H. P. Hratchian, A. F. Izmaylov, J. Bloino, G. Zheng, J. L. Sonnenberg, M. Hada, M. Ehara, K. Toyota, R. Fukuda, J. Hasegawa, M. Ishida, T. Nakajima, Y. Honda, O. Kitao, H. Nakai, T. Vreven, J. A. Montgomery, J. E. Peralta, F. Ogliaro, M. Bearpark, J. J. Heyd, E. Brothers, K. N. Kudin, V. N. Staroverov, T. Keith, R. Kobayashi, J. Normand, K. Raghavachari, A. Rendell, J. C. Burant, S. S. Iyengar, J. Tomasi, M. Cossi, N. Rega, J. M. Millam, M. Klene, J. E. Knox, J. B. Cross, V. Bakken, C. Adamo, J. Jaramillo, R. Gomperts, R. E. Stratmann, O. Yazyev, A. J. Austin, R. Cammi, C. Pomelli, J. W. Ochterski, R. L. Martin, K. Morokuma, V. G. Zakrzewski, G. A. Voth, P. Salvador, J. J. Dannenberg, S. Dapprich, A. D. Daniels, O. Farkas, J. B. Foresman, J. V. Ortiz, J. Cioslowski and D. J. Fox, *Gaussian 09 (Revision B.01)*, Gaussian Inc., Wallingford, CT, 2010.
48 D. C. Carter and J. X. Ho, *Adv. Protein Chem.*, 1994, **45**, 153–203.
49 G. Sudlow, D. J. Birkett and D. N. Wade, *Mol. Pharmacol.*, 1976, **12**, 1052–1061.
50 K. Tang, Y.-M. Qin, A.-H. Lin, X. Hu and G.-L. Zou, *J. Pharm. Biomed. Anal.*, 2005, **39**, 404–410.
51 S. N. Khana, B. Islama, R. Yennamalli, A. Sultana, N. Subbarao and A. U. Khana, *Eur. J. Pharm. Sci.*, 2008, **35**, 371–382.
52 G. M. Morris, R. Huey, W. Lindstrom, M. F. Sanner, R. K. Below, D. S. Goodsell and A. Olson, *J. Comput. Chem.*, 2009, **30**, 2785–2791.
53 V. Barone and M. Cossi, *J. Phys. Chem. A*, 1998, **102**, 1995–2001.
54 M. Cossi, N. Rega, G. Scalmani and V. Barone, *J. Comput. Chem.*, 2003, **24**, 669–681.
55 J. I. Aihara, *J. Phys. Chem. A*, 1999, **103**, 7487–7495.
56 R. G. Pearson, *Hard and soft acids and bases*, Dowden, Hutchinson, Ross, Stroudsburg, PA, 1973.
57 R. G. Pearson, *J. Chem. Educ.*, 1987, **64**, 561–567.
58 M. Grossl, E. Reisner, C. G. Hartinger, R. Eichinger, O. Semenova, A. R. Timerbaev, M. A. Jakupec, V. B. Arion and B. K. Keppler, *J. Med. Chem.*, 2007, **50**, 2185–2193.

